

Multicontinuum homogenization in perforated domains

Wei Xie¹, Yalchin Efendiev², Yunqing Huang³, Wing Tat Leung⁴, and Yin Yang⁵

¹National Center for Applied Mathematics in Hunan, Xiangtan University, Xiangtan 411105, Hunan, China. xiew@smail.xtu.edu.cn

²Department of Mathematics, Texas A&M University, College Station, TX 77843, USA; efendiev@math.tamu.edu

³School of Mathematics and Computational Science, Xiangtan University, Xiangtan 411105, Hunan, China huangyq@xtu.edu.cn

⁴Department of Mathematics, City University of Hong Kong, Hong Kong; sidnet123@gmail.com

⁵School of Mathematics and Computational Science, Xiangtan University, Xiangtan 411105, Hunan, China yangyinxtu@xtu.edu.cn

Abstract

In this paper, we develop a general framework for multicontinuum homogenization in perforated domains. The simulations of problems in perforated domains are expensive and, in many applications, coarse-grid macroscopic models are developed. Many previous approaches include homogenization, multiscale finite element methods, and so on. In our paper, we design multicontinuum homogenization based on our recently proposed framework. In this setting, we distinguish different spatial regions in perforations based on their sizes. For example, very thin perforations are considered as one continua, while larger perforations are considered as another continua. By differentiating perforations in this way, we are able to predict flows in each of them more accurately. We present a framework by formulating cell problems for each continuum using appropriate constraints for the solution averages and their gradients. These cell problem solutions are used in a multiscale expansion and in deriving novel macroscopic systems for multicontinuum homogenization. Our proposed approaches are designed for problems without scale separation. We present numerical results for two continuum problems and demonstrate the accuracy of the proposed methods.

1 Introduction

Problems in perforated domains appear in many applications. These include subsurface applications, materials science, membranes, filters, and so on. Simulations at the pore scale are very expensive and require gridding entailing a very large number of degrees of freedom. In many applications, researchers would like to perform simulations on a coarse grid and obtain models that do not include perforations. These coarse grid models have been a topic of interest for many years. In this paper, we propose some novel algorithms for simulations in perforated domains.

Some of the first approaches for modeling on a coarse grid include homogenization methods, e.g., Darcy's law. In these approaches, one assigns an effective property to each representative volume based on local simulations. These effective properties are then used to form coarse-grid equations. Homogenization techniques are specifically designed for problems in perforated domains

[19, 11, 12, 13, 22]. In these techniques, the solution is expanded using a two-scale ansatz, and the terms in the expansion are computed via substitution. In many applications, the homogenized equation is derived on a coarse grid and does not contain oscillations, while the homogenized coefficients are computed based on local cell solutions.

An alternative approach is the use of multiscale methods. In these approaches, the solution is sought on a coarse grid using multiscale basis functions, which are solutions of local problems and are computed locally. In [15, 16, 18], the authors propose Multiscale Finite Element Method (MsFEM) approaches, where a limited number of basis functions via local solutions are computed, and the accuracy and robustness of the approach are demonstrated. In [9, 4, 6, 8, 7, 5], the authors propose multiscale enrichment and design the Generalized Multiscale Finite Element Method (GMsFEM). In these approaches, multiscale basis construction is proposed and analyzed. By adding additional multiscale basis functions on the pore scale, the accuracy of the coarse-grid simulation improves. In further generalization [3, 2], the authors propose the Constraint Energy Minimizing Generalized Multiscale Finite Element Method (CEM-GMsFEM) approach. In this approach, multiscale basis functions are constructed in oversampled regions using constraints. It can be shown that the accuracy of these approaches is independent of small scales.

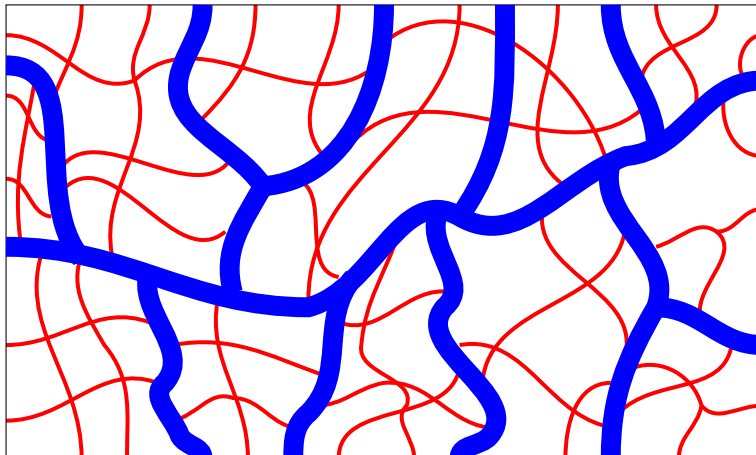


Figure 1: Illustration of two continua (red and blue).

In our paper, we utilize the concept of multicontinuum homogenization proposed in [10]. The main idea of multicontinuum homogenization is to formulate a coarse-grid equation using constraint cell problems. These approaches borrow some ideas from CEM-GMsFEM; however, their goal is to derive macroscopic equations and identify macroscopic variables that smoothly vary over the spatial region. In multicontinuum homogenization, one deals with problems where multiple macroscopic media are present. In this case, we consider perforated domains with vastly different perforation sizes (see Fig. 1). Such perforated media arise in many applications, where one deals with vastly different sizes of regions, for example, blood vessels, perforation sizes, fractures, vugs, and so on. In these problems, it is more advantageous to separate the two media, as the solution in each type of perforation (small and large) can behave drastically differently. Indeed, if the effects of these perforations are lumped into one average across both small and large perforations, then the effects

of small perforations will be ignored, as their effects are much weaker compared to those in large ones. For this reason, we propose a multicontinuum approach for such homogenization that can handle problems without scale separation.

Some of the main ingredients of the proposed approach are the use of constraint cell problems and multicontinuum homogenization expansion. In our approach, we propose cell problem formulations that are constrained in different parts of the perforations. More precisely, our cell problems constrain averages and gradients of the solution in subregions of perforations. These cell problems are used in a multiscale multicontinuum expansion. By substituting this expansion into the macroscale equation, we derive a system of equations that describe the coarse-grid system.

One of the main differences between our approach and multiscale methods is that the proposed methods provide a coarse-grid model in the form of differential equations. This is because we seek smooth functions that can approximate the coefficients in multiscale numerical approaches and can formulate macroscopic models for these global coarse-grid smooth solutions. We perform numerical experiments for Laplace's equation in perforated domains, even though our approach can be used for other applications. We choose several types of perforated domains that include thick and small channels, representing two continua. We solve the cell problems and compute the effective properties. Effective properties are directional and larger if more channels are in the corresponding direction. We compare the coarse-grid solution to the averaged fine-grid solutions. The averages are taken in each subregion. Our numerical results show that the errors are small, and the macroscopic model accurately predicts the averages of the fine-grid solution.

Our contributions in this paper are as follows:

- Development of a framework for multicontinuum homogenization in perforated regions by identifying various continua regions.
- Formulation of multicontinuum constraint cell problems and multiscale expansion.
- Derivation of macroscopic equations in the form of coupled convection-diffusion-reaction equations.
- Presentation of numerical results for various types of multicontinua media.

The paper is organized as follows. In Section 2, we present preliminaries. Section 3 is devoted to the description of multicontinua approach. The numerical results are presented in Section 4. We make some conclusions in Section 5.

2 Preliminaries

In this section, we present the model problem and review some previous work. Consider the following equations in a perforated domain,

$$\mathcal{L}(u) = f \text{ in } \Omega^\epsilon, \tag{1}$$

subject to some boundary and initial conditions. Here, ϵ denotes multiscale quantities, such as domains or variables, and $\Omega \subset \mathbb{R}^d$ (with $d = 2, 3$) is a bounded domain. Let \mathcal{B}^ϵ be the set of perforations within Ω , and define $\Omega^\epsilon = \Omega \setminus \mathcal{B}^\epsilon$.

To simplify the notations, let $V(\Omega^\epsilon)$ be the appropriate solution space, and

$$V_0(\Omega^\epsilon) = \{v \in V(\Omega^\epsilon), v = 0 \text{ on } \partial\Omega^\epsilon\}.$$

The variational formulation of (1) is to find $u \in V(\Omega^\epsilon)$ such that

$$(\mathcal{L}(u), v)_{\Omega^\epsilon} = (f, v)_{\Omega^\epsilon}, \quad \forall v \in V_0(\Omega^\epsilon),$$

where (\cdot, \cdot) denotes a specific inner product for scalar functions or vector functions in the perforated domain Ω^ϵ . In the following, we provide two examples for the abstract notations.

1. For the Laplace operator,

$$\mathcal{L}(u) = -\Delta u, \tag{2}$$

we assume the boundary conditions is homogeneous Dirichlet.

2. For Stokes equations, we have

$$\mathcal{L}(u, p) = \begin{pmatrix} \nabla p - \mu \Delta u \\ \nabla \cdot u \end{pmatrix}, \tag{3}$$

where μ is the viscosity, p is the fluid pressure, u represents the velocity.

Next, we review some related techniques for multiscale modeling for problems in perforated domains. These include homogenization, MsFEM, GmsFEM techniques and their variations.

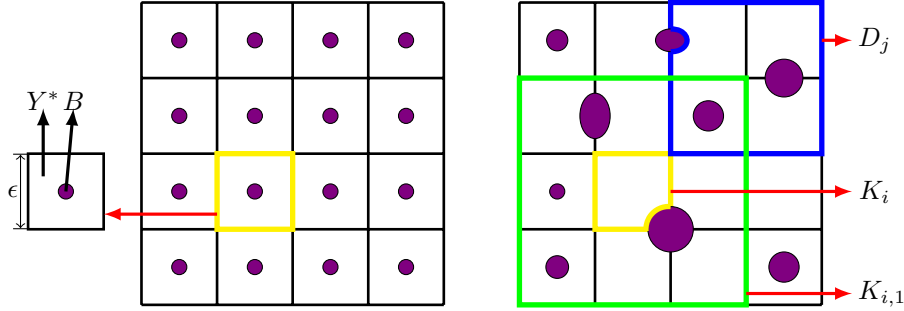


Figure 2: Left: Periodic perforated domain Ω^ϵ . Right: Non-periodic perforated domain.

2.1 Homogenization

In this subsection, we briefly review homogenization techniques and refer to [14, 20]. We assume the perforations are periodic (see Fig. 2). In this context, ϵ represents the period of the perforations. For a given cell Y , we denote the perforated region as B , and define the remaining part within Ω^ϵ as $Y^* = Y \setminus B$.

In homogenization, we obtain macroscopic equations using two-scale expansion that are formulated in the whole domain without perforations

$$\mathcal{L}^*(u^*) = f \quad \text{in } \Omega, \tag{4}$$

where \mathcal{L}^* is the macroscopic operator. The form of the macroscopic operator depends on microscopic equations. For example, for Laplace operator,

$$\mathcal{L}^*(u^*) = -\nabla \cdot (a_{ij}^* \nabla u^*),$$

where

$$a_{ij}^* = \int_{Y^*} \delta_{ij} + \partial_{y_i} w_j(\mathbf{y}) \, d\mathbf{y},$$

and w_j satisfied $-\Delta w_j = 0$ in Y^* . On the other hand, for Stokes equations, the macroscopic equations differ from the microscopic equations and have the following form

$$\mathcal{L}^*(u^*, p^*) = \begin{pmatrix} \operatorname{div}(u^*) \\ u^* + a_{ij}^* \nabla p^* \end{pmatrix}$$

where $a_{ij}^* = \int_{Y^*} w_j \cdot e^i = \int_{Y^*} \nabla w_i : \nabla w_j$, w_j is the cell solution of the following problem,

$$\begin{cases} -\mu \Delta w_j + \nabla p_j = e_j, & \text{in } Y^*, \\ \operatorname{div}(w_j) = 0, & \text{in } Y^*, \\ w_j = 0, & \text{on } \partial B. \end{cases}$$

2.2 Multiscale finite element method

Another class of approaches involves the use of multiscale basis functions. In these methods, multiscale finite element basis functions are constructed to solve the problem on a coarse grid. As detailed in [16, 17], the MsFEM approach can be employed to address non-periodic scenarios, as illustrated in Fig. 2. Let \mathcal{T}^H denote a uniform mesh that partitions the domain Ω , where K_i represents the coarse cell corresponding to the portion within Ω^ϵ , i.e., $K_i \subset \Omega^\epsilon$. Besides, we use E_j to denote the coarse edge, and \mathcal{E} is the set of all E_j .

For Laplace equations on the fine grid, we need to construct the local basis functions as shown in (5), where \mathbf{x}_j are coarse vertices in Ω^ϵ .

$$\begin{cases} -\Delta \phi_j = 0, & \text{in } K_i, \\ \phi_j = \mu_j, & \text{on } \partial K_i. \end{cases} \quad (5)$$

where μ_j represents some boundary conditions, as described in [15]. Additionally, more basis functions are required to address the absence of coarse vertices not included in Ω^ϵ .

$$\begin{cases} -\Delta \psi_i = 1, & \text{in } K_i, \\ \psi_i = 0, & \text{on } \partial K_i. \end{cases} \quad (6)$$

2.3 Generalized multiscale finite element method

For the Generalized Multiscale Finite Element Method (GMsFEM), an extension beyond the single basis function paradigm of MsFEM is available, as outlined in [5]. Similar to the MsFEM framework, we employ a rectangular mesh \mathcal{T}^H to partition the domain Ω . Here, D_j represent the support of multiscale basis functions the same as the MsFEM.

For the snapshot space, we generally have two options. The first option is to use all fine-grid basis functions, while the other option is to solve the following equations.

$$\begin{cases} \mathcal{L}(\psi_l^{\text{snap}}) = 0, & \text{in } D_i, \\ \psi_l^{\text{snap}} = \delta_l^h, & \text{on } \partial D_i. \end{cases} \quad (7)$$

The snapshot space in D_i is defined as $V^{\text{snap}}(D_i) = \text{span}_l\{\psi_l^{\text{snap}}\}$. Then, we need use a spectrum problem to reduce the dimension of the local snapshot space,

$$a_i(\psi_j^i, v) = \lambda_j^i s_i(\psi_j^i, v), \quad \forall v \in V^{\text{snap}}(D_i). \quad (8)$$

In here, $s_i(u, v) = \int_{D_i} \tilde{\kappa} uv$, and $a_i(u, v) = \int_{D_i} \nabla u \cdot \nabla v$ for Laplace problem (2), while $a_i(u, v) = \int_{D_i} \nabla u : \nabla v$ for Stokes equations (3). By selecting the smallest l_i eigenvalues, the eigenfunctions will construct the offline space. At last, the multiscale space is construct by the combination of partition unity and offline space,

$$V_{\text{ms}} = \text{span}_{i,j}\{\chi_i \psi_j^i\}.$$

2.4 Constraint energy minimizing Generalized multiscale finite element method

For Constraint energy minimizing - Generalized multiscale finite element method (CEM-GMsFEM), we need two steps to construct the multiscale space, refer to [2, 21].

First, we need to construct a auxiliary space, solving (9) in a coarse cell K_i ,

$$a_i(\phi_j^i, v) = \lambda_j^i s_i(\phi_j^i, v), \quad \forall v \in V(K_i). \quad (9)$$

and select the first l_i smallest eigenvalues and corresponding eigenfunctions. In here, $s_i(u, v) = \int_{K_i} \tilde{\kappa} uv$, and $a_i(u, v) = \int_{K_i} \nabla u \cdot \nabla v$ for Laplace problem (2) and $a_i(u, v) = \int_{K_i} \nabla u : \nabla v$ for Stokes equations (3). We can define the local auxiliary space, $V_{\text{aux}}^i = \text{span}\{\phi_i^1, \dots, \phi_i^{l_i}\}$. The global inner product $a(\cdot, \cdot)$, $s(\cdot, \cdot)$ is the sum of each K_i , we can also define a global operator $\pi : H_0^1(\Omega^\epsilon) \rightarrow V_{\text{aux}}$,

$$\pi(u) = \sum_{i=1}^{N_c} \sum_{j=1}^{l_i} \frac{s_i(u, \phi_j^i)}{s_i(\phi_j^i, \phi_j^i)} \phi_j^i, \quad \forall u \in V.$$

The multiscale basis functions need to solve a minimization problem.

1. For Laplace equations,

$$\psi_{j,\text{ms}}^i = \text{argmin}\{a(\psi, \psi) + s(\pi(\psi) - \phi_j^i, \pi(\psi) - \phi_j^i) \mid \psi \in V_0(K_{i,m_i})\}. \quad (10)$$

2. For Stokes problem,

$$\psi_{j,\text{ms}}^i = \text{argmin}\{a(\psi, \psi) + s(\pi(\psi) - \phi_j^i, \pi(\psi) - \phi_j^i) \mid \psi \in V_0(K_{i,m_i}) \text{ and } \nabla \cdot \psi = 0\}. \quad (11)$$

The multiscale space is $V_{\text{ms}} = \text{span}_{i,j}\{\psi_{j,\text{ms}}^i\}$.

3 Multicontinuum homogenization

In this section, we introduce the model problem and outline the fundamental concept of the multi-continuum homogenization method applied to perforated domains.

In our study, we define $\mathcal{L}(\cdot) = -\text{div}(\kappa \nabla \cdot)$ in Equation (1), subject to homogeneous Dirichlet boundary conditions:

$$\begin{cases} -\text{div}(\kappa \nabla u) = f, & \text{in } \Omega^\epsilon, \\ u = 0, & \text{on } \partial\Omega^\epsilon. \end{cases} \quad (12)$$

Similar to the homogenization example presented in Section 2, we assume that the perforations \mathcal{B}^ϵ exhibit some periodicity in Equation (12). Here, we use ϵ to represent the periodicity, which corresponds to the width of a single structure. In applications, channels of different widths may possess varying capabilities in transporting flow. Thus, we categorize continua based on the width of the channels. In this paper, we focus on the two-continua method, as illustrated in Figure 3. Specifically, we use two distinct colors to denote different channels, where blue represents thick channels and red indicates thin channels. It's worth noting that this method can be easily extended to handle multi-channel scenarios.

The weak formulation of Equation (12) is given by:

$$a(u, v) = (f, v), \quad \forall v \in H_0^1(\Omega^\epsilon), \quad (13)$$

where

$$a(u, v) = \int_{\Omega^\epsilon} \kappa \nabla u \nabla v, \quad (f, v) = \int_{\Omega^\epsilon} f v.$$

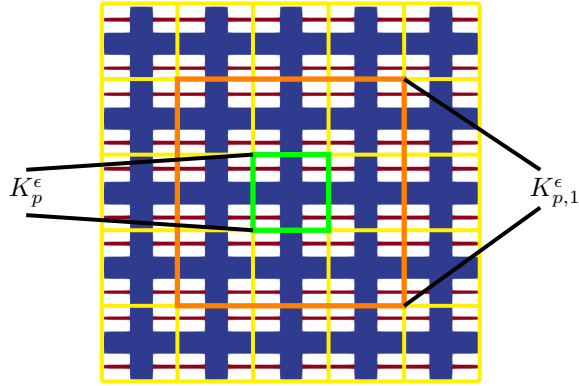


Figure 3: Illustration.

Before presenting the computation, let's review the computational mesh. We denote a coarse block in the partition of the domain Ω as K , with a diameter much larger than the heterogeneities, i.e., larger than the smallest size of the regions. Use N_c to denote the number of coarse grid. Similar to CEM-GMsFEM, we extend the coarse block K_p by l coarse blocks, denoted by $K_{p,l}$. We use K^ϵ to represent the computational domain within K , defined as $K^\epsilon = \Omega^\epsilon \cap K$. Additionally, we

introduce $K_{p,l}^\epsilon$ as the remaining part of the oversampled domain $K_{p,l}$ in Ω^ϵ , which may contain more local geometric information, as illustrated in Figure 3. To distinguish between different continua, we define the characteristic function for continuum i as ψ_i , satisfying $\psi_i = \delta_{ij}$ within continuum j .

In the multicontinuum homogenization method, we postulate that the solution u can be expressed as a series expansion of macroscopic variables U_i . Typically, due to the non-periodic nature of geometric configurations or coefficients within the operator, such as permeability κ , local information ϕ must be computed within each coarse block K_p^ϵ . It is crucial to emphasize that while the variable U_i is defined across the global domain Ω , the local information ϕ_i is confined to Ω^ϵ . We represent the solution u as follows:

$$u = \phi_i U_i + \phi_i^m \partial_m U_i + \phi_i^{mn} \partial_{mn}^2 U_i + \dots, \quad (14)$$

where $\partial_m = \frac{\partial}{\partial x_m}$, $\partial_{mn}^2 = \frac{\partial^2}{\partial x_m \partial x_n}$. In general, we consider only the average and the gradient,

$$u \approx \phi_i U_i + \phi_i^m \partial_m U_i. \quad (15)$$

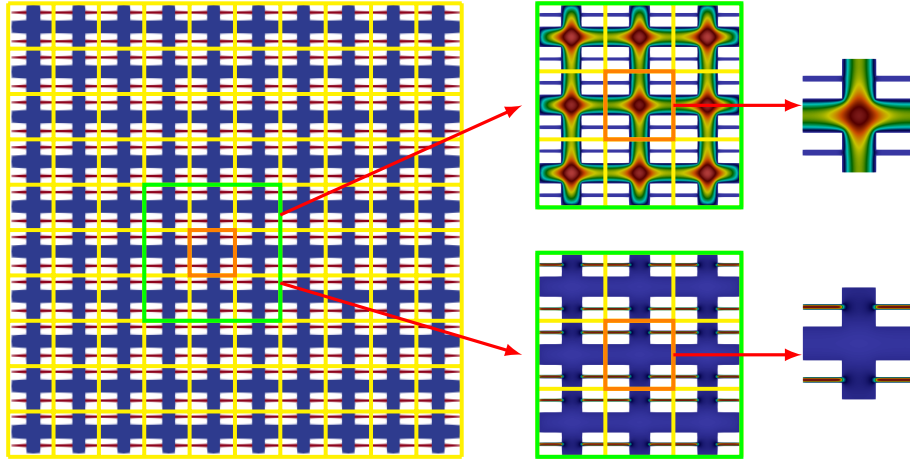


Figure 4: Illustration of the computational process for a cell problem.

The construction of local information ϕ_i is divided into N_c local problems, as depicted in Fig. 4. Here, we denote $\phi_i|_{K_p^\epsilon} = \phi_i^p$. Subsequently, the superscript p will be omitted, as local computation will be performed for each coarse block K_p^ϵ , i.e., $\phi_i|_{K_p^\epsilon} = \phi_i$. From previous work [10, 1], it's evident that the cell problem is crucial for obtaining an accurate macroscopic equation. These cell problems are typically formulated by constraining the original equation within an oversampled domain $K_{p,l}^\epsilon$. Our first cell problem imposes constraints to represent the constants in the average behavior of each continuum.

$$\begin{aligned} \int_{K_{p,l}^\epsilon} \kappa \nabla \phi_i \cdot \nabla v - \sum_{j,q} \frac{\beta_{ij}^q}{\int_{K_q^\epsilon} \psi_j} \int_{K_q^\epsilon} \psi_j v &= 0, \\ \int_{K_q^\epsilon} \phi_i \psi_j &= \delta_{ij} \int_{K_q^\epsilon} \psi_j. \end{aligned} \quad (16)$$

Our second cell problem imposes constraints to represent the linear functions in the average behavior of each continua.

$$\begin{aligned} \int_{K_{p,l}^\epsilon} \kappa \nabla \phi_i^m \cdot \nabla v - \sum_{j,q} \frac{\beta_{ij}^{mq}}{\int_{K_q^\epsilon} \psi_j} \int_{K_q^\epsilon} \psi_j v &= 0, \\ \int_{K_q^\epsilon} \phi_i^m \psi_j &= \delta_{ij} \int_{K_q^\epsilon} (x_m - c_{mj}) \psi_j. \end{aligned} \quad (17)$$

where c_{mj} satisfy $\int_{K_p^\epsilon} (x_m - c_{mj}) \psi_j = 0$. It's important to note that (16) and (17) will use the zero Dirichlet boundary condition, meaning that ϕ 's are all zero on $\partial K_{p,l}^\epsilon$, which is consistent with the original boundary conditions. The oversampling technique aims to remove the boundary effect, but we still need to constrain ϕ 's in K_p^ϵ .

Following the above assumption, we only consider the average and gradient of macroscopic variables. In particular, we have:

$$\begin{aligned} u &\approx \phi_i U_i + \phi_i^m \partial_m U_i, \\ v &\approx \phi_j V_j + \phi_j^m \partial_m V_j. \end{aligned} \quad (18)$$

Substituting (18) into (13), we obtain the following equation:

$$\begin{aligned} a(\phi_i U_i, \phi_j V_j) + a(\phi_i U_m, \phi_j^n \partial_n V_j) + a(\phi_i^m \partial_m U_i, \phi_j V_j) \\ + a(\phi_i^m \partial_m U_i, \phi_j^n \partial_n V_j) &= (f, \phi_j V_j) + (f, \phi_j^n \partial_n V_j). \end{aligned} \quad (19)$$

Define an local inner product $a_p(u, v) = \int_{K_p^\epsilon} \kappa \nabla u \cdot \nabla v$. Considering U_i and V_i as macroscopic variables, they can be taken out of the integrals over K . Thus, we have:

$$\begin{aligned} a(\phi_i, \phi_j) U_i V_j + a(\phi_i, \phi_j^n) U_i \partial_n V_j + a(\phi_i^m, \phi_j) \partial_m U_i V_j \\ + a(\phi_i^m, \phi_j^n) \partial_m U_i \partial_n V_j &= (f, \phi_j) V_j + (f, \partial_n \phi_j) \partial_n V_j. \end{aligned} \quad (20)$$

In Equation (20), considering that U_i and V_i are smooth functions defined in Ω , we derive the following macroscopic equation for U_i (in strong form):

$$B_{ji} U_i + B_{ji}^m \partial_m U_i - \partial_n \bar{B}_{ji}^n U_i - \partial_n (B_{ji}^{mn} \partial_m U_i) = b_j, \quad (21)$$

where the coefficients are piecewise-constant vectors or matrices, we have:

$$\begin{aligned} B_{ji} &= a(\phi_i, \phi_j), \quad B_{ji}^m = a(\phi_i^m, \phi_j) \\ \bar{B}_{ji}^n &= a(\phi_i, \phi_j^n), \quad B_{ji}^{mn} = a(\phi_i^m, \phi_j^n), \quad b_j = (f, \phi_j). \end{aligned} \quad (22)$$

Ultimately, we only need to solve (21) in Ω to obtain the macroscopic solution. It's important to note:

1. A suitable oversampling layer can mitigate the boundary effects; achieving high accuracy typically requires only one or two layers. This is attributed to our knowledge of the interior boundary conditions and the properties of the macroscopic equation.
2. The concept of the Representative Volume Element (RVE) remains applicable in this context.

4 Numerical results

In this section, we conduct numerical experiments to examine the behavior of two different media with varying conductivity (κ) using four examples. The source term will be fixed at $f = 5\pi^2 \sin(2\pi x_1) \sin(\pi x_2)$. The computation domain is $\Omega = [0, 1]^2$. Unlike previous studies, we adopt a coarse mesh size H equivalent to the periodicity parameter ϵ , which is also the diameter of a single structure. We will use a fine mesh size of $H/80$ to solve the reference solution.

To measure the efficiency of our method, we define the relative L^2 -error in Ω_1 and the relative L^2 -error in Ω_2 as:

$$e_2^{(i)} = \frac{\sum_p \left| \frac{1}{|K_p|} \int_{K_p} U_i - \frac{1}{|K_p^\epsilon \cap \Omega_i|} \int_{K_p^\epsilon \cap \Omega_i} u \right|^2}{\sum_p \left| \frac{1}{|K_p^\epsilon \cap \Omega_i|} \int_{K_p^\epsilon \cap \Omega_i} u \right|^2}.$$

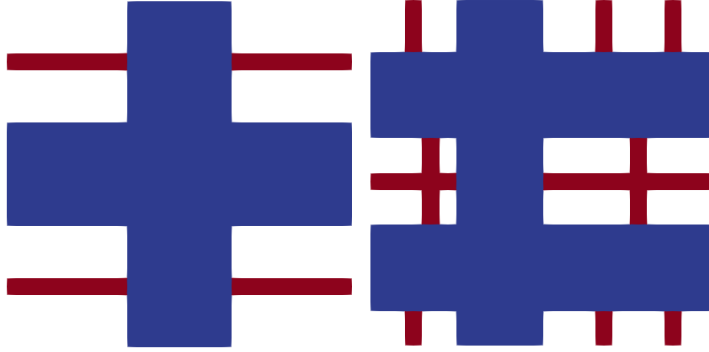


Figure 5: Left: single structure 1. Right: single structure 2.

4.1 Case 1

In this example, we take $\kappa = 1$, and use structure 1 as the single structure. We depict the fine-grid solution in Fig. 6, while the corresponding averaged solution in Fig. 7. From Fig. 7, we conclude that our method provides an accurate approximation of the averaged solution. In Table 1, we observe that the error will decay very fast with the coarse mesh size decrease. Besides, we find that achieving high accuracy only requires oversampling one coarse layer. In Table 2, we present some coefficient in macroscopic equation, which can demonstrate the relationship between error and oversampling layers.

4.2 Case 2

In this example, we keep $\kappa = 1$ and utilize structure 2 different as Case 1. We present the solution obtained from the fine-grid approach in Fig. 8, alongside the corresponding averaged solution displayed in Fig. 9. From the analysis of Fig. 9, we infer that our method yields a precise approximation of the averaged solution. The data in Table 3 indicates a rapid decay in error as the coarse

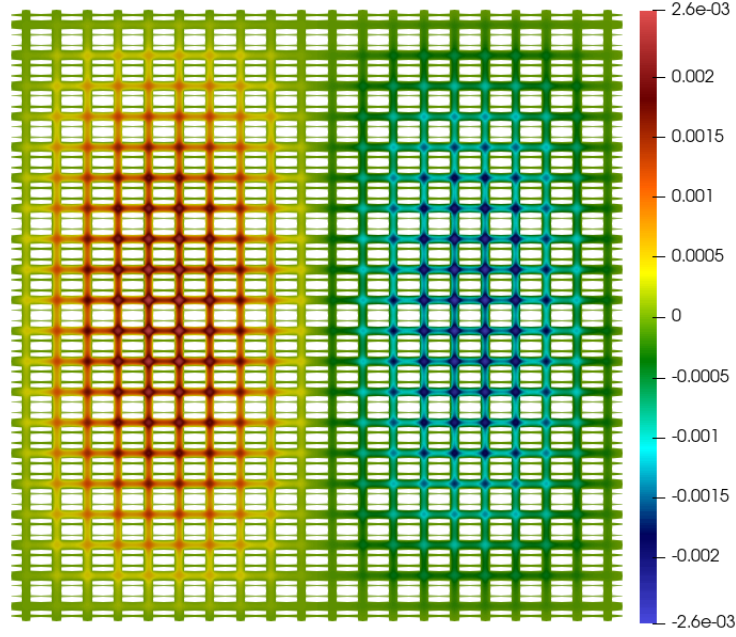


Figure 6: Reference solution for Case 1.

l	$\epsilon = 1/10$		$\epsilon = 1/20$		$\epsilon = 1/40$	
	$e_2^{(1)}$	$e_2^{(2)}$	$e_2^{(1)}$	$e_2^{(2)}$	$e_2^{(1)}$	$e_2^{(2)}$
0	4.22e-02	1.04e-02	3.32e-02	5.29e-03	3.12e-02	4.31e-03
1	2.12e-03	1.94e-03	1.43e-04	1.22e-04	9.91e-06	7.85e-06
2	2.04e-03	1.93e-03	1.35e-04	1.21e-04	8.89e-06	7.73e-06

Table 1: Relative error in different continuum when use structure 1 and set $\kappa = 1$.

l	B_{11}	B_{12}	B_{22}
0	60.70	-2.00	383.59
1	50.10	-1.81	365.83
2	50.10	-1.81	365.82

Table 2: Homogenization coefficient in Case 1.

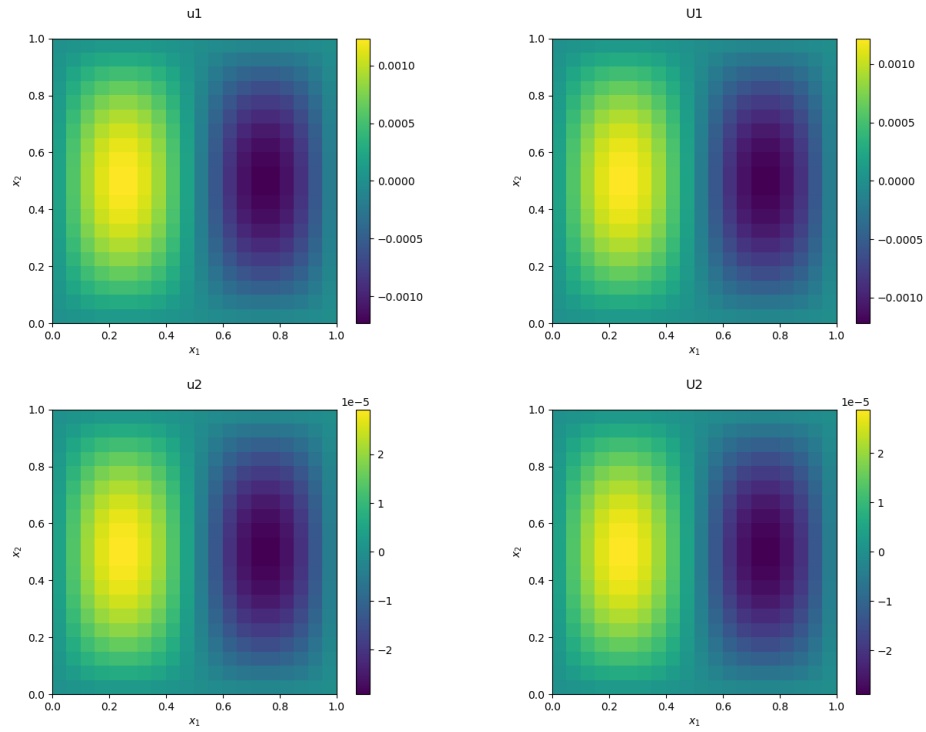


Figure 7: Average solution for Case 1. Top Left: Reference averaged solution in Ω_1 . Top Right: Multiscale average solution in Ω_1 . Bottom Left: Reference averaged solution in Ω_2 . Bottom Right: Multiscale average solution in Ω_2 .

mesh size decreases. Moreover, we find that achieving high accuracy only requires oversampling one coarse layer. Table 4 provides coefficients in the macroscopic equation, aiding the error will converge with only 1 oversampling layer.

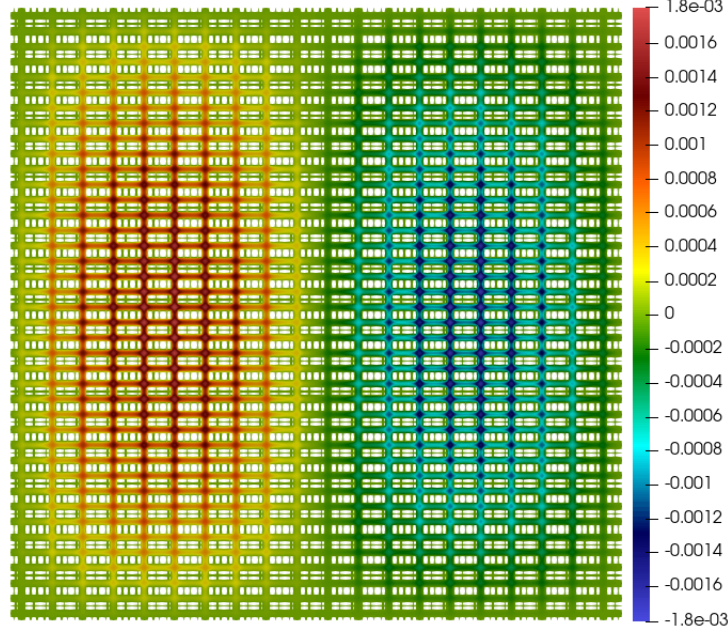


Figure 8: Reference solution for Case 2.

l	$\epsilon = 1/10$		$\epsilon = 1/20$		$\epsilon = 1/40$	
	$e_2^{(1)}$	$e_2^{(2)}$	$e_2^{(1)}$	$e_2^{(2)}$	$e_2^{(1)}$	$e_2^{(2)}$
0	3.81e-02	1.17e-02	2.93e-02	6.36e-03	2.73e-02	5.30e-03
1	2.26e-03	1.94e-03	1.57e-04	1.23e-04	1.13e-05	7.97e-06
2	2.17e-03	1.92e-03	1.47e-04	1.21e-04	1.02e-05	7.77e-06

Table 3: Relative error in different continuum when use structure 2 and set $\kappa = 1$.

4.3 Case 3

In this example, we take a slow variable coefficient, $\kappa = 2 + \sin(\pi x_1) \sin(\pi x_2)$. The structure 1 is used for the single structure. We present the fine-scale solution in Fig. 10. In Fig. 12, we can see that our method can provides an accurate approximation of the averaged solution. Different with the last two examples, we depicted the homogenization coefficient in Fig. 11. In Table 5, we note that the error will decay with the reduce the coarse mesh size.

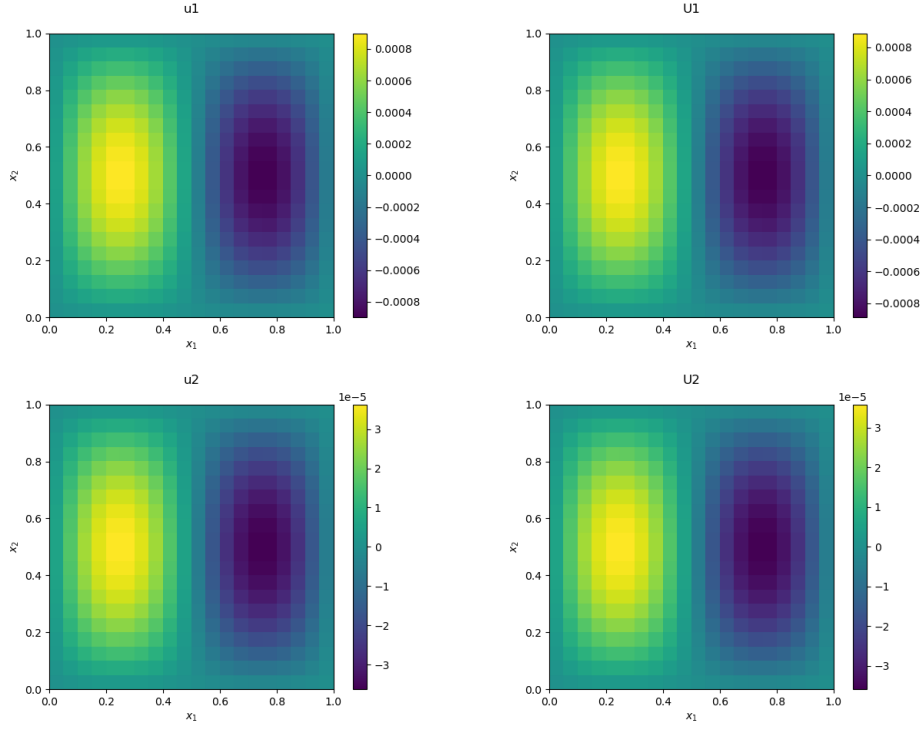


Figure 9: Average solution for Case 2. Top Left: Reference averaged solution in Ω_1 . Top Right: Multiscale average solution in Ω_1 . Bottom Left: Reference averaged solution in Ω_2 . Bottom Right: Multiscale average solution in Ω_2 .

l	B_{11}	B_{12}	B_{22}
0	101.10	-6.92	494.14
1	84.57	-5.93	462.72
2	84.57	-5.93	462.72

Table 4: Homogenization coefficient in Case 2.

l	$\epsilon = 1/10$		$\epsilon = 1/20$		$\epsilon = 1/40$	
	$e_2^{(1)}$	$e_2^{(2)}$	$e_2^{(1)}$	$e_2^{(2)}$	$e_2^{(1)}$	$e_2^{(2)}$
0	4.20e-02	1.02e-02	3.31e-02	5.25e-03	3.11e-02	4.30e-03
1	2.10e-03	1.90e-03	1.39e-04	1.18e-04	9.58e-06	7.54e-06
2	2.02e-03	1.89e-03	1.31e-04	1.17e-04	8.57e-06	7.42e-06

Table 5: Relative error in different continuum when use structure 1 and set $\kappa = 2 + \sin(\pi x_1) \sin(\pi x_2)$.

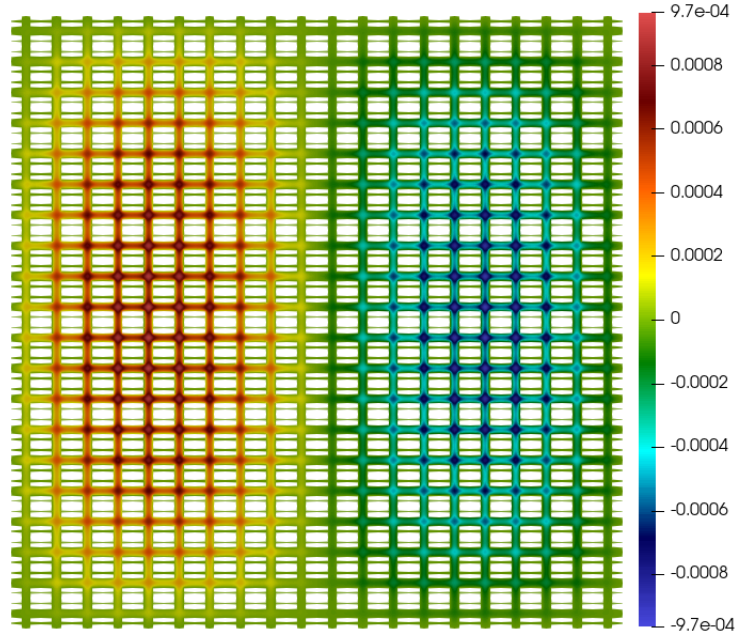


Figure 10: Reference solution for Case 3.

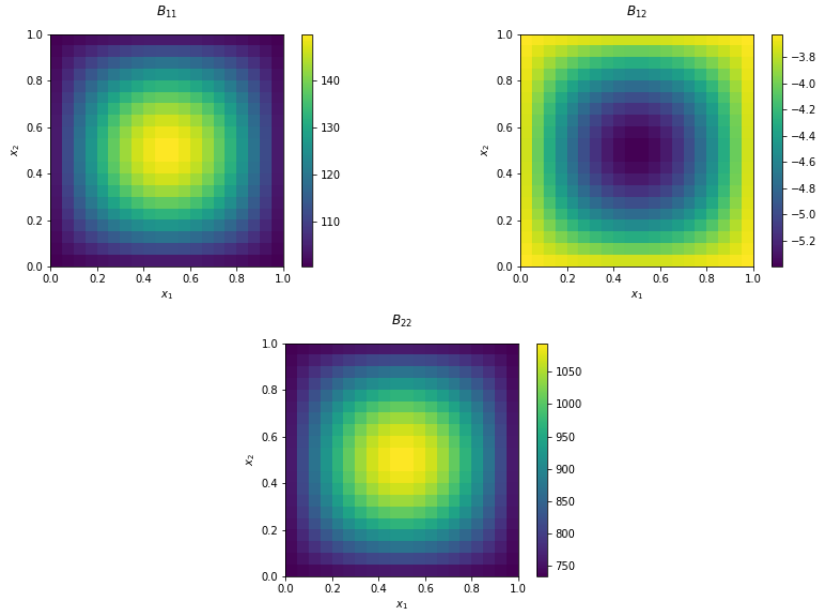


Figure 11: Homogenization coefficient for Case 3. From Left to Right and Top to Bottom: B_{11}, B_{12}, B_{22} .

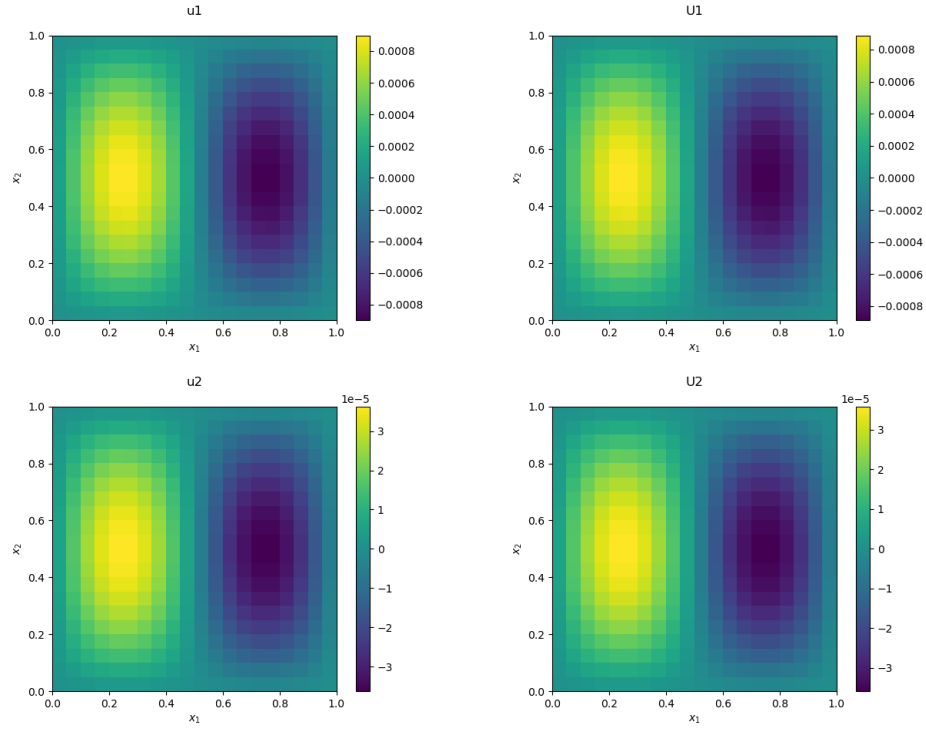


Figure 12: Average solution for Case 3. Top Left: Reference averaged solution in Ω_1 . Top Right: Multiscale average solution in Ω_1 . Bottom Left: Reference averaged solution in Ω_2 . Bottom Right: Multiscale average solution in Ω_2 .

4.4 Case 4

In this example, we set $\kappa = 2 + \sin(\pi x_1) \sin(\pi x_2)$ and utilize Structure 2 as the single structure. The fine-grid solution is depicted in Fig. 13, while the reference averaged solution and multicontinuum homogenization solution are presented in Fig. 14. The figures further demonstrate the efficiency of our method. In Table 6, we show the error by varying the periodic and oversampling layers. We observe that the error decays very rapidly when decreasing the periodicity. Additionally, in Fig. 15, we show the homogenization coefficients.

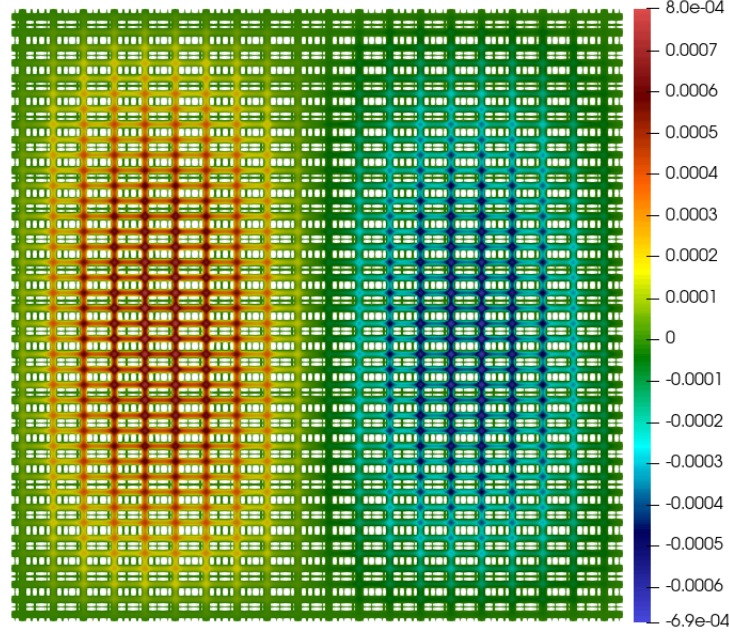


Figure 13: Reference solution for Case 4.

l	$\epsilon = 1/10$		$\epsilon = 1/20$		$\epsilon = 1/40$	
	$e_2^{(1)}$	$e_2^{(2)}$	$e_2^{(1)}$	$e_2^{(2)}$	$e_2^{(1)}$	$e_2^{(2)}$
0	3.79e-02	1.17e-02	2.92e-02	6.36e-03	2.73e-02	5.30e-03
1	2.20e-03	1.95e-03	1.55e-04	1.23e-04	1.13e-05	7.96e-06
2	2.11e-03	1.93e-03	1.45e-04	1.21e-04	1.02e-05	7.75e-06

Table 6: Relative error in different continuum when use structure 2 and set $\kappa = 2 + \sin(\frac{\pi x_1}{2}) \sin(\frac{\pi x_2}{2})$.

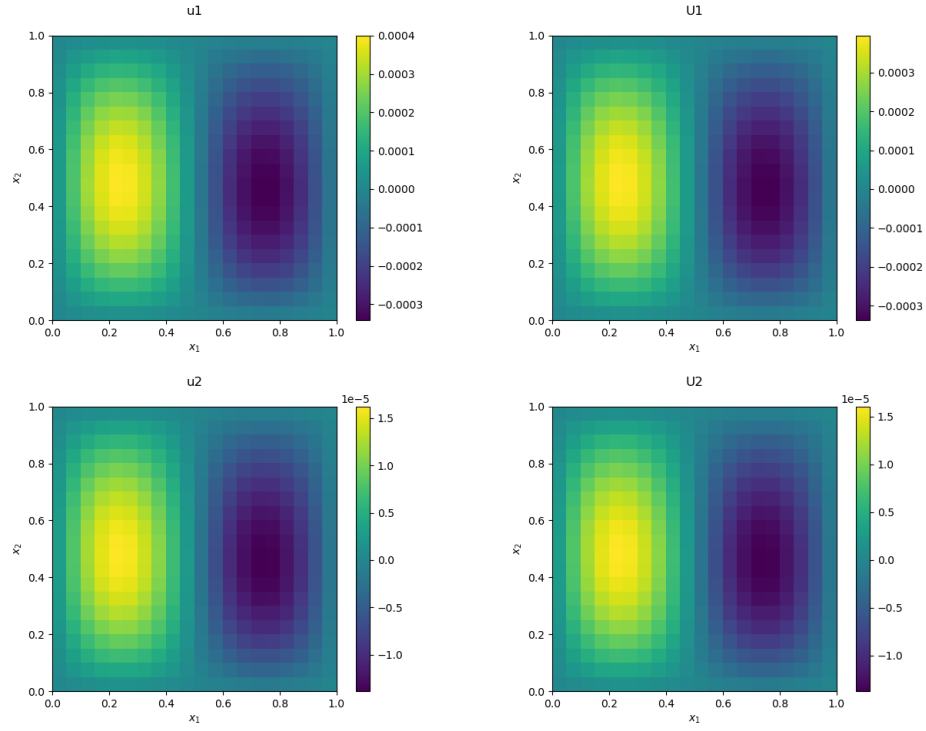


Figure 14: Average solution for Case 4. Top Left: Reference averaged solution in Ω_1 . Top Right: Multiscale average solution in Ω_1 . Bottom Left: Reference averaged solution in Ω_2 . Bottom Right: Multiscale average solution in Ω_2 .

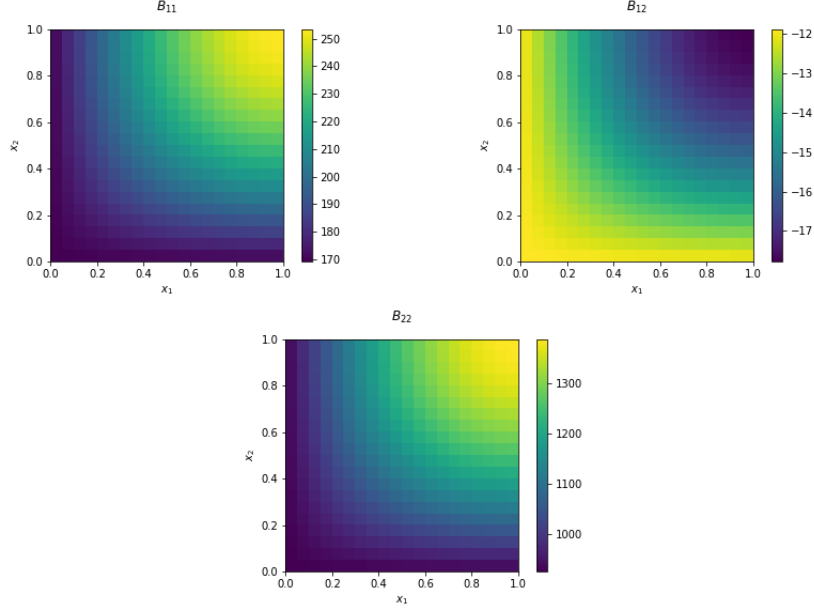


Figure 15: Homogenization coefficient for Case 4. From Left to Right and Top to Bottom: B_{11}, B_{12}, B_{22} .

5 Conclusions

In this paper, we propose a multicontinuum homogenization approach for problems in perforated domains. The perforated regions are divided into subregions, where each subregion is treated as a separate continua due to their size differences. Typically, different continua may have significantly different widths or lengths. We formulate constraint cell problems by imposing constraints in subregions for the averages of the solutions and their gradients. Using the cell solutions, we formulate a homogenization expansion and derive macroscopic equations. The resulting macroscopic equations consist of a system of equations. We present numerical results by considering two continua media with significantly different widths. We consider various diffusion scenarios, and our numerical results show very good accuracy.

Acknowledgement

WX and YY were supported by the National Natural Science Foundation of China Project (12071402, 12261131501), the Project of Scientific Research Fund of the Hunan Provincial Science and Technology Department (2022RC3022). WTL is supported by Early Career Award, Research Grant Council, Project Number: 21307223. YE would like to thank the partial support from NSF 2208498.

References

- [1] E Chung, Y Efendiev, J Galvis, and WT Leung. Multicontinuum homogenization. general theory and applications. *arXiv preprint arXiv:2309.08128*, 2023.
- [2] Eric Chung, Jiuhua Hu, and Sai-Mang Pun. Convergence of the cem-gmsfem for stokes flows in heterogeneous perforated domains. *Journal of Computational and Applied Mathematics*, 389:113327, 2021.
- [3] Eric T Chung, Yalchin Efendiev, and Wing Tat Leung. Constraint energy minimizing generalized multiscale finite element method. *Computer Methods in Applied Mechanics and Engineering*, 339:298–319, 2018.
- [4] Eric T Chung, Yalchin Efendiev, Wing Tat Leung, Maria Vasilyeva, and Yating Wang. Online adaptive local multiscale model reduction for heterogeneous problems in perforated domains. *Applicable Analysis*, 96(12):2002–2031, 2017.
- [5] Eric T Chung, Yalchin Efendiev, Guanglian Li, and Maria Vasilyeva. Generalized multiscale finite element methods for problems in perforated heterogeneous domains. *Applicable Analysis*, 95(10):2254–2279, 2016.
- [6] Eric T Chung, Wing Tat Leung, and Maria Vasilyeva. Mixed gmsfem for second order elliptic problem in perforated domains. *Journal of Computational and Applied Mathematics*, 304:84–99, 2016.
- [7] Eric T Chung, Wing Tat Leung, Maria Vasilyeva, and Yating Wang. Multiscale model reduction for transport and flow problems in perforated domains. *Journal of Computational and Applied Mathematics*, 330:519–535, 2018.
- [8] Eric T Chung, Maria Vasilyeva, and Yating Wang. A conservative local multiscale model reduction technique for stokes flows in heterogeneous perforated domains. *Journal of Computational and Applied Mathematics*, 321:389–405, 2017.
- [9] Yalchin Efendiev, Juan Galvis, and Thomas Y Hou. Generalized multiscale finite element methods (gmsfem). *Journal of computational physics*, 251:116–135, 2013.
- [10] Yalchin Efendiev and Wing Tat Leung. Multicontinuum homogenization and its relation to nonlocal multicontinuum theories. *Journal of Computational Physics*, 474:111761, 2023.
- [11] Patrick Henning and Mario Ohlberger. The heterogeneous multiscale finite element method for elliptic homogenization problems in perforated domains. *Numerische Mathematik*, 113:601–629, 2009.
- [12] Matthieu Hillairet. On the homogenization of the stokes problem in a perforated domain. *Archive for Rational Mechanics and Analysis*, 230:1179–1228, 2018.
- [13] Ulrich Hornung. *Homogenization and porous media*, volume 6. Springer Science & Business Media, 1997.
- [14] Ulrich Hornung. *Homogenization and porous media*, volume 6. Springer Science & Business Media, 2012.

- [15] Thomas Y Hou and Xiao-Hui Wu. A multiscale finite element method for elliptic problems in composite materials and porous media. *Journal of computational physics*, 134(1):169–189, 1997.
- [16] Claude Le Bris, Frédéric Legoll, and Alexei Lozinski. An msfem type approach for perforated domains. *Multiscale Modeling & Simulation*, 12(3):1046–1077, 2014.
- [17] Yong Lu. Uniform estimates for stokes equations in a domain with a small hole and applications in homogenization problems. *Calculus of Variations and Partial Differential Equations*, 60:1–31, 2021.
- [18] Bagus Putra Muljadi, Jacek Narski, Alexei Lozinski, and Pierre Degond. Nonconforming multiscale finite element method for stokes flows in heterogeneous media. part i: methodologies and numerical experiments. *Multiscale Modeling & Simulation*, 13(4):1146–1172, 2015.
- [19] E Weinan and Bjorn Engquist. The heterogenous multiscale methods. *Communications in Mathematical Sciences*, 1(1):87–132, 2003.
- [20] Sylvain Wolf. Homogenization of the stokes system in a non-periodically perforated domain. *Multiscale Modeling & Simulation*, 20(1):72–106, 2022.
- [21] Wei Xie, Yin Yang, Eric Chung, and Yunqing Huang. Cem-gmsfem for poisson equations in heterogeneous perforated domains.
- [22] GA Yosifian. On some homogenization problems in perforated domains with nonlinear boundary conditions. *Applicable Analysis*, 65(3-4):257–288, 1997.